Investigation of Domain Formation in Sphingomyelin/Cholesterol/POPC Mixtures by Fluorescence Resonance Energy Transfer and Monte Carlo Simulations

Monica L. Frazier, Jenny R. Wright, Antje Pokorny, and Paulo F. F. Almeida
Department of Chemistry and Biochemistry, University of North Carolina Wilmington, Wilmington, North Carolina 28403

ABSTRACT We have recently proposed a phase diagram for mixtures of porcine brain sphingomyelin (BSM), cholesterol (Chol), and 1-palmitoyl-2-oleoyl-phosphatidylcholine (POPC) on the basis of kinetics of carboxyfluorescein efflux induced by the amphipathic peptide δ-lysin. Although that study indicated the existence of domains, phase separations in the micrometer scale have not been observed by fluorescence microscopy in BSM/Chol/POPC mixtures, though they have for some other sphingomyelins (SM). Here we examine the same BSM/Chol/POPC system by a combination of fluorescence resonance energy transfer (FRET) and Monte Carlo simulations. The results clearly demonstrate that domains are formed in this system. Comparison of the FRET experimental data with the computer simulations allows the estimate of lipid-lipid interaction Gibbs energies between SM/Chol, SM/POPC, and Chol/POPC. The latter two interactions are weakly repulsive, but the interaction between SM and Chol is favorable. Furthermore, those three unlike lipid interaction parameters between the three possible lipid pairs are sufficient for the existence of a closed loop in the ternary phase diagram, without the need to involve multibody interactions. The calculations also indicate that the largest POPC domains contain several thousand lipids, corresponding to linear sizes of the order of a few hundred nanometers.

INTRODUCTION

The formation of domains in ternary mixtures of sphingomyelin (SM), 1-palmitoyl-2-oleoyl-phosphatidylcholine (POPC), and cholesterol (Chol) has received considerable attention. Phase diagrams of membranes containing these three components have been investigated experimentally (1–3) and theoretically (4,5) because those lipids are the major components of the outer monolayer of mammalian membranes (6,7) and are believed to be essential components of membrane rafts (8–18).

Using the terminology of liquid-liquid phase separation first introduced by Ipsen et al. (19,20), POPC forms a liquid-disordered (L_d) phase, whereas SM/Chol mixtures with a molar ratio close to 1:1 form a liquid-ordered (L_o) phase (21–24). The existence of phases or domains in ternary mixtures and the location of their boundaries in the phase diagram have been somewhat controversial (1,25), but there is fairly good agreement on the broad location of a region of L_d/L_o coexistence at room temperature, as depicted in Fig. 1. The exact location, shape, and boundaries of this L_d/L_o coexistence region appear to vary with the method of observation and the precise type of SM and phosphatidylcholine (PC) (1–3). Nevertheless, some form of L_d/L_o coexistence appears to be a general feature of mixtures containing equimolar amounts of SM and Chol, with variable amounts of PC (Fig. 1, *dashed line*). It seems that a significant part of the discrepancies lies in the spatial resolution of the various methods used. In particular, giant unilamellar vesicles (GUVs) prepared from mixtures containing brain sphingomyelin (BSM) appear uniform by fluorescence microscopy (26) but seem to consist of different lipid domains when examined by other methods. We could not explain the kinetics of interaction of the peptide δ-lysin with vesicles of BSM/Chol/POPC in any other way than through L_d/L_o domain coexistence (1,27). For domains to be visible by fluorescence microscopy, their size must be larger than the wavelength of the light used, in practice typically of the order of 1 μm. Fluorescence resonance energy transfer (FRET) has indicated the existence of domains in mixtures where they are not detected by fluorescence microscopy (25,28,29).

Another point much debated in the field is whether phospholipid/Chol interactions are best described as L_d/L_o domain (or phase) coexistence or as condensed complexes of phospholipid and Chol (13,30). Here, Monte Carlo simulations of a simple lattice model of the membrane are used to help in understanding the microscopic behavior of these mixtures. If one focuses on the L_d/L_o coexistence region (Fig. 1), SM and POPC are both in a liquid state. Therefore, no phase transitions are involved, and each lipid can be represented by a single state. POPC is envisioned to be in the L_d state and SM in the L_o state. The Gibbs energy of the lattice is determined solely by differences in the mutual interactions of lipid neighbors. The unlike nearest-neighbor interaction Gibbs energy (31), or interaction parameter for short, is defined for each pair of lipids (A, B = SM, POPC, or Chol, A ≠ B) by

Submitted October 30, 2006, and accepted for publication December 18, 2006.

Address reprint requests to Paulo F. F. Almeida, Dept. of Chemistry and Biochemistry, University of North Carolina Wilmington, Wilmington, NC 28403. Tel.: 910-962-7300; Fax: 910-962-3013; E-mail: almeidap@uncw.edu.

0006-3495/07/04/2422/12 $2.00

doi: 10.1529/biophysj.106.100107

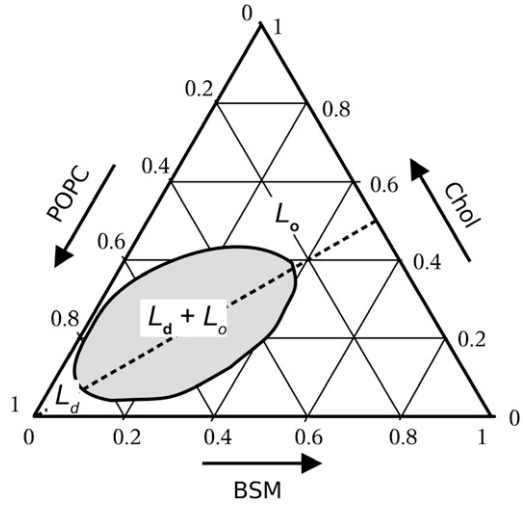

FIGURE 1 Simplified phase diagram for a ternary mixture of BSM/Chol/POPC at ~25°C, based on kinetics of peptide/membrane interactions (1). The approximate location of the L_d/L_o coexistence region is shown in gray. Detailed diagrams have been published for a few mixtures (1–3). Most of these diagrams show a central two-phase, L_d/L_o coexistence region, which in some systems appears more complicated because of the presence of adjacent regions containing solid phases (1,2).

$$\omega_{AB} = g_{AB} - \frac{1}{2}(g_{AA} + g_{BB}), \quad (1)$$

where g_{AA} and g_{BB} are the Gibbs energies of interaction between two A or two B molecules, and g_{AB} is the Gibbs energy of interaction between one A and one B molecule. It is the parameter ω_{AB} that determines whether lipids A and B mix well or separate into domains. Therefore, the most important decision in this type of Monte Carlo simulation is the choice of unlike nearest-neighbor interaction parameters. In this system, there are three: ω_{SP} for SM/POPC, ω_{SC} for SM/Chol, and ω_{CP} for Chol/POPC interactions. These parameters can be estimated from experimental lipid distributions obtained using the nearest-neighbor recognition method of Regen (32,33). Briefly, a binary mixture containing lipid analogs with a thiol group is allowed to reach its equilibrium distribution under conditions where thiolate/disulfide exchange occurs. The mixture is then quenched by changing to acidic conditions, fixing the disulfide bonds between analog lipid pairs. Several types of lipid dimers are thus formed: A-B heterodimers and two types of homodimers, A-A and B-B. The distribution of heterodimers and homodimers is then analyzed and the equilibrium constant for partner exchange is calculated. These types of data have been obtained for several lipid pairs (34–38). From those data, ω_{AB} for different pairs of lipids can be calculated (31,39). Another approach is to obtain an experimental measure of domain formation, from FRET or excimer/monomer ratios (40,41), and compare it with Monte Carlo simulations, varying ω_{AB} in the simulations until a match is obtained. Similarly, the experimental data can be obtained from the heat capacity functions of pure and mixed bilayers, which are compared with those calculated from Monte Carlo simulations (42–44). In has been found that for most lipid pairs $\omega_{AB} = \pm 100$–300 cal/mol (31), which is at most half the thermal energy at room temperature, k_BT, where k_B is Boltzmann's constant. For reference, close to room temperature, a value of $\omega_{AB} = +400$ cal/mol in a two-component system leads to complete phase separation (45). Most unlike lipid-lipid interactions are found to be repulsive ($\omega_{AB} > 0$), meaning that lipids prefer to interact with like neighbors, but some are attractive ($\omega_{AB} < 0$) (31). The interaction between saturated PC and Chol is especially important. Zhang et al. (39) studied the temperature dependence of the unlike nearest-neighbor interaction Gibbs energy between dipalmitoylphosphatidylcholine (DPPC) and Chol in the L_o phase, where the Chol content is high. This temperature dependence of ω_{AB} for DPPC/Chol corresponds to an interaction enthalpy of -2 kcal/mol (39). From those data, $\omega_{AB} = -320$ cal/mol is estimated at 20°C, in the L_o phase. For distearoylphosphatidylcholine (DSPC) and Chol, using a similar temperature dependence of the interaction parameter as for DPPC/Chol in combination with high temperature measurements (31,37), the interaction between DSPC and Chol is estimated to be $\omega_{AB} = -350$ cal/mol.

It is well established that in the L_o state the interaction between SM and Chol is at least as favorable as between long-chain saturated PC and Chol (9,46–48). Therefore, it appears reasonable that the interaction parameter between SM and Chol be close to the largest value for PC/Chol in the L_o phase, that is, $\omega_{SC} = -350$ cal/mol. The interaction between Chol and saturated PC in the L_d state is close to ideal ($\omega_{AB} \approx 0$) (31,37,39). However, Chol interacts less favorably with unsaturated PC (46), to the point of showing a strong 'aversion' to polyunsaturated PC (49). The interaction of Chol with POPC must therefore lie between these two situations. It is not clear whether L_d-L_o phase separation between Chol and POPC exists at all. Some reports favor its existence (2,25,50), but others do not (1,3,51). Most likely, if it exists, it is not extensive (1). Also, increasing ω_{AB} to 330 cal/mol between gel and fluid DPPC lipids leads to a first-order phase transition (52), setting an upper bound for the value of ω_{CP}. Therefore, a value of ω_{CP} in the range 100–200 cal/mol appears appropriate. The results reported here were obtained with $\omega_{CP} = 200$ cal/mol for the POPC/Chol interaction. Finally, for the interaction between POPC and SM a small value would be appropriate if the system were entirely in the L_d state. But for mixtures in the L_d/L_o coexistence region of the phase diagram, there is always a high content of Chol, so that most of the SM is probably in the L_o state. SM and POPC exhibit a large region of gel/L_d phase separation (1). A value of $\omega_{SP} = 300$ cal/mol appears reasonable, as it is intermediate between the onset of large-scale phase separation ($\geq$330 cal/mol) and almost ideal mixing ($<$200 cal/mol) (40). The physical origins of these lipid-lipid interactions were discussed in a recent review (31).

In this article, FRET between a novel donor/acceptor pair of fluorescent lipids is used to investigate the existence of domains in BSM/Chol/POPC mixtures. This is combined with Monte Carlo simulations of the lipid bilayer on a lattice to obtain a measure of the lipid-lipid interactions between these three components. The simulations indicate the presence of domains on the order of a few hundred nanometers in addition to many smaller ones. These sizes would be below the resolution of fluorescence microscopy. Further, the Monte Carlo simulations are in good agreement with the FRET experimental data if a favorable interaction parameter of -350 cal/mol between SM and Chol is used. This is a strong interaction for a lipid pair and would be consistent with formation of SM/Chol condensed complexes. On the other hand, the simulations also reveal the formation of large domains of mainly POPC and others of mainly SM/Chol, which can be identified with the L_d and L_o phases.

METHODS

Chemicals

1-Palmitoyl-2-oleoyl-*sn*-glycero-3-phosphocholine (POPC), 1-palmitoyl-2-oleoyl-*sn*-glycero-3-phosphoserine (POPS), and 1-palmitoyl-2-oleoyl-*sn*-glycero-3-phosphoethanolamine (POPE) in chloroform solution; SM ((2S,3R,4E)-2-acylaminooctadec-4-ene-3-hydroxy-1-phosphocholine) from porcine brain (BSM), in chloroform solution; and Chol, as powder, were purchased from Avanti Polar Lipids (Alabaster, AL). The fatty acid chain composition of BSM, specified by the vendor, is the following: 16:0 (2%), 18:0 (49%), 20:0 (5%), 22:0 (8%), 24:0 (6%), 24:1 (20%), and other chains (10%). 4-Chloro-7-nitrobenz-2-oxa-1,3-diazole (NBD-Cl) and 1-[[(6,8-difluoro-7-hydroxy-4-methyl-2-oxo-2H-1-benzopyran-3-yl)acetyl]oxy]-succinimidyl ester (Marina Blue-succinimidyl ester, MB-SE) were purchased from Molecular Probes/Invitrogen (Carlsbad, CA). Organic solvents (high-performance liquid chromatography/American Chemical Society (ACS) grade) were purchased from Burdick & Jackson (Muskegon, MI). Lipids and probes were tested by thin-layer chromatography (TLC) and used without further purification.

Preparation of large unilamellar vesicles

Large unilamellar vesicles (LUVs) were prepared by mixing the appropriate lipid amounts in 4:1 chloroform ($CHCl_3$)/methanol (MeOH) in a round-bottom flask. The solvent was rapidly evaporated using a rotary evaporator (Büchi R-3000, Flawil, Switzerland) at 60°C–70°C. The lipid film was then placed under vacuum for 4–8 h and hydrated at room temperature for POPC and POPS and at 70°C for the mixtures containing BSM by the addition of buffer containing 20 mM MOPS (3-(*N*-morpholino)propanesulfonic acid), pH 7.5, 0.1 mM EGTA, 0.02% NaN_3, and 100 mM KCl. The suspension was then extruded 10 times through two stacked Nuclepore polycarbonate filters (Whatman, Florham, NJ) of 0.1-μm pore size, using a water-jacketed high pressure extruder from Lipex Biomembranes (Vancouver, Canada) at room temperature for POPC and POPS and at 70°C for the mixtures containing BSM. Lipid concentrations were assayed by the Bartlett phosphate method (53), modified as previously described (54), with the absorbance read at 580 nm. Lipid vesicles were kept in the dark under nitrogen at room temperature.

Synthesis of fluorescent probes

The synthesis of NBD-POPE and MB-POPE were performed as described generally by Vaz and Hallmann (55), with the following specific procedures. Organic solvents were dried with molecular sieves (Sigma-Aldrich, St. Louis, MO). POPE solutions in $CHCl_3$ were first dried in a rotary evaporator and the lipid film was then dissolved in ~0.5 mL of dry $CHCl_3$. A total of ~5 mg of NBD-Cl or MB-SE were reacted in a probe/lipid ratio of ~1:1.1 with POPE. MB-SE was dissolved in ~0.3 mL dry dimethylformamide (DMF); NBD-Cl solid was dissolved in ~0.3 mL dry $CHCl_3$/MeOH 1:1 (v/v). Crushed K_2CO_3, dried for 24 h at 80°C and then kept desiccated, was added to the POPE solution in a 1.1:1 salt/lipid ratio. The probe (MB or NBD) solution was then added drop-wise to the POPE/K_2CO_3 solution. The reaction mixtures were stirred in the dark and analyzed by TLC using dichloromethane (CH_2Cl_2)/MeOH 2:1 for MB and CH_2Cl_2/MeOH/water 65:25:4 for NBD. The reaction took ~1–3 h for completion for MB-SE and ~4–6 h for NBD-Cl. The fluorescent probes were identified with ultraviolet light and the phosphorus-containing lipids with the Zinzade reaction (56). Purification was performed on preparatory TLC using CH_2Cl_2/MeOH 4:1. The products were eluted from the silica using CH_2Cl_2/MeOH 2:1, after which the solvent was rotary-evaporated at 50°C. Finally, the products (MB-POPE or NBD-POPE) were dissolved in a minimal amount of dry $CHCl_3$ and kept under nitrogen at -30°C. Absorbances were determined in MeOH (basic for MB) in a CARY 1E ultraviolet-visible spectrophotometer (Varian, Australia), and lipid concentrations were determined by the Bartlett phosphate assay (53).

FRET measurements

Fluorescence measurements were performed in a SLM-Aminco 8100 spectrofluorimeter (Urbana, IL). MB was excited at 367 nm and the emission wavelength was scanned from 380 to 600 nm. The slitwidths were 2 nm (excitation) and 8 nm (emission). FRET from MB to NBD was measured as described in detail in the Results section.

The overlap integral (57) was calculated from

$$J(\lambda) = \frac{\int_0^\infty F_D(\lambda)\varepsilon_A(\lambda)\lambda^4\, d\lambda}{\int_0^\infty F_D(\lambda)\, d\lambda}, \quad (2)$$

where $F_D(\lambda)$ is the fluorescence emission of the donor (MB) and $\varepsilon_A(\lambda)$ is the absorption of the acceptor (NBD). The Förster distance, which is the distance between the donor and acceptor fluorophores that corresponds to 50% energy transfer efficiency is then obtained from $J(\lambda)$ by (57)

$$R_0 = 0.211[\kappa^2 n^{-4} Q_D J(\lambda)]^{1/6}, \quad (3)$$

where κ^2 is the relative orientational factor between dipoles, n is the refractive index of the medium, Q_D is the quantum yield of the donor, and the numerical factor combines unit conversion factors (57). κ^2 can vary between 0–4 and we used the standard approach of taking $\kappa^2 = 2/3$, which is the motion-averaged value. For the refractive index of a vesicle suspension the value of $n = 1.4$ was used (57). The quantum yield of MB is $Q_D = 0.89$ (58), and the extinction coefficient of NBD-POPE at 463 nm is $\varepsilon_A = 21{,}000$ M^{-1} cm^{-1} (59). The calculated Förster distance was $R_0 = 46$ Å. For reference, we determined $\varepsilon_A = 24{,}000$ M^{-1} cm^{-1} for MB-POPE at 368 nm (absorption maximum) under basic conditions (methanol/~50 mM KOH).

Monte Carlo simulations

Monte Carlo simulations were performed on a Linux workstation with in-house FORTRAN code programs using the NAG f95 compiler (Numerical Algorithms Groups, Oxford, UK). The lipid bilayer was represented by two superimposed triangular lattices with skew-periodic boundary conditions (60). Lattices of 100×100 sites were used in most simulations. To verify that the conclusions apply to the experimental system employed (LUV, with ~10^5 lipids) a few simulations were performed on a 300×300 lattice (9×10^4 sites). Each lattice represents one of the leaflets of the bilayer and each site represents a lipid molecule, SM, POPC, or Chol. Phospholipids are

considered to be in a liquid state for the compositions simulated, according to the phase diagram (Fig. 1). Therefore, no phase transitions are involved. POPC is envisioned to be in the L_d state and SM in the L_o state, but this conceptual framework has no influence on the simulations. The energy of the lattice is determined solely by differences in the mutual interactions of lipid neighbors. These interactions are represented by unlike nearest-neighbor interaction Gibbs energies, or interaction parameters for short, ω_{AB}, defined for each pair of lipids (A, B = SM, POPC, or Chol, A $\neq$ B) by Eq. 1. The equilibration of the lattice is achieved by site exchange using a variation on the method of Kawasaki (61). Rather than exchanging only nearest neighbors, the two sites for which a switch is attempted are both picked randomly from anywhere in the lattice. This ensures a much faster equilibration of the system and has no effect on the equilibrium properties calculated. This method could not be used for realistic kinetics because diffusion in a real system occurs by exchange of lipid nearest neighbors. However, the interest here is only in equilibrium properties, and allowing for exchange of nonnearest neighbors is a much more efficient equilibration method. The reason is, if only exchange of nearest neighbors is attempted, after small domains form a large fraction of the attempted moves leads to no change because there is a high probability that two neighbors are identical. This results in a waste of calculation time. In any case, simulations that used only nearest-neighbor exchange were also performed and the results were identical to those that used nonnearest neighbor exchanges—but the time to reach equilibrium was $\sim$10$\times$ longer.

The algorithm is as follows. A Monte Carlo cycle (mcc) is defined as a number of attempted moves equal to the lattice size (10^4 for a 100 $\times$ 100 lattice). For each attempted move, a site on the lattice is picked at random. Here and in all other cases, the random number generator *ran2* of Press et al. (62) was used. The site to exchange with the first picked site is also chosen at random. The Gibbs energies before and after the exchange are calculated and the exchange probability is defined by $p = \exp(-\Delta G/k_BT)$, where k_B is Boltzmann's constant and T is temperature, which was set to 300 K in all simulations. The acceptance of the move is based on the algorithm of Metropolis et al. (63): if $p \geq 1$ the move is accepted; if $p < 1$, a random number (*Ran#*) is generated, and the move is accepted if $p >$ *Ran#*. The simulations were run for 10^5 mcc, which ensured that equilibrium was reached, as confirmed by occasional longer runs. The most important average properties computed were the POPC domain size and the fluorescence energy transfer efficiency (E_t).

To the best of our knowledge, the partition coefficient (K_p) of NBD-POPE between SM/Chol and POPC bilayers has never been determined. For NBD-dimyristoylphosphatidylethanolamine (DMPE), $K_p = 5.9$ in favor of POPC over SM/Chol 6:4, and $K_p = 4.2$ in favor of POPC/Chol 1:1 over SM/Chol 6:4 (64). Based on its much lower T_m, NBD-POPE is expected to partition even more favorably into POPC over SM/Chol mixtures. However, rather than assuming a value for K_p in the simulations, we simply assume that the fluorescent lipid probes, MB-POPE and NBD-POPE, behave as tagged POPC molecules in their interactions with other lipids. The only difference is that they can transfer energy if an acceptor (NBD-POPE) is within the distance R_0 of a donor (MB-POPE). This assumption appears entirely justified because the acyl chains of both probes are exactly the same as those of POPC. Furthermore, experimentally there was no difference in FRET in bilayers of POPC or POPS, which have the same acyl chains. Therefore, the headgroup difference appears to have little influence in this respect.

Since a lipid has a diameter of $\sim$8 Å, the experimentally determined $R_0 =$ 46 Å corresponds to a circle with a radius of $\sim$6 lipids (Fig. 2). The energy transfer efficiency, $E_t = R_0^6/(R_0^6+r^6)$, as a function of distance, r, is replaced in the Monte Carlo simulations by a step function. Thus, a donor is considered to transfer energy if at least one acceptor is found within a distance of 6 lipids on the lattice in the same leaflet of the bilayer. Energy transfer across the bilayer occurs over a projected distance of $\sim$2 lipids in the opposite leaflet. This follows from the assumption that the fluorophore moieties of the probes occupy a location approximately equal to that occupied by the choline groups and knowing that the distance between the choline headgroups in dioleoylphosphatidylcholine is $\sim$42 Å (65). In the algorithm, energy is always transferred if an acceptor resides within R_0 from a donor after one mcc. The only adjustable parameters in the simulations were the unlike lipid-lipid interaction Gibbs energies between unlike nearest neighbors (ω_{AB}).

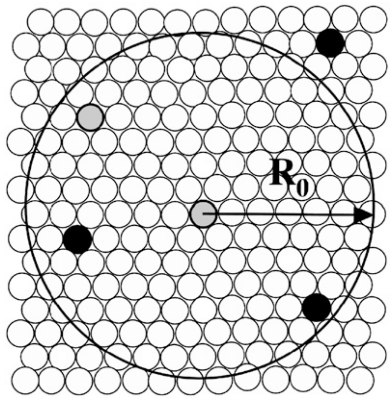

FIGURE 2 Schematic representation of the definition of the Monte Carlo lattice and the Förster distance R_0. Open circles represent lattice sites (lipids: BSM, POPC, or Chol). Solid circles represent FRET acceptors (NBD-POPE) and gray circles represent FRET donors (MB-POPE). Energy transfer is considered to occur if an acceptor is found within the radius R_0 of a donor. The proportion of probes to lipids represented is about the same as used in the experiments and in the simulations.

RESULTS

Characterization of energy transfer

The absorption spectra of MB-POPE (in alkaline methanol) and NBD-POPE (in methanol), and the fluorescence emission spectra of MB-POPE and NBD-POPE incorporated in POPC vesicles in buffer at pH 7.5 are shown in Fig. 3. It is apparent

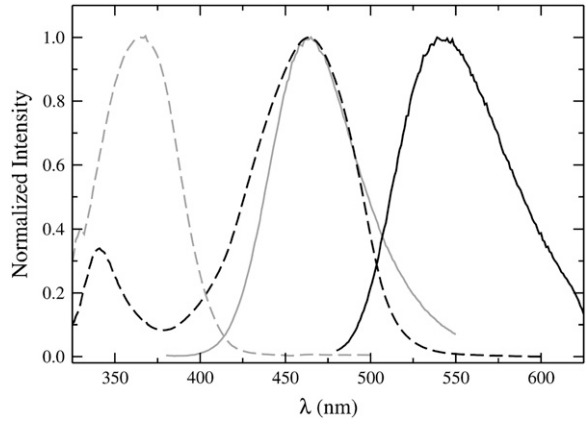

FIGURE 3 Absorption and fluorescence emission spectra of MB-POPE and NBD-POPE. Absorption spectra were recorded in methanol (alkaline solution for MB-POPE). Emission spectra were recorded in aqueous buffer at pH 7.5, in POPC vesicles (100 μM) containing 10 mol % of either fluorescent probe. The gray lines correspond to the absorption (*dashed*) and emission (*solid*) spectra of MB-POPE. The black lines correspond to the absorption (*dashed*) and emission (*solid*) spectra of NBD-POPE.

that a large overlap exists between the emission of MB-POPE and the absorption of NBD-POPE. Therefore, these two fluorophores constitute an excellent Förster energy transfer pair. This is the first time its use is reported, to the best of our knowledge. The overlap integral was calculated from those spectra according to Eq. 2 to yield a value of $R_0 = 46$ Å using Eq. 3.

Relation between FRET and peak ratio

When measuring energy transfer, a significant portion of the error arises from the determination of lipid concentrations. Typically, a sample containing both donor and acceptor and another sample containing only donor are prepared and the efficiency of energy transfer (E_t) is obtained, upon donor excitation, from the ratio of donor fluorescence in the presence of acceptor (F_{DA}) to donor fluorescence in the absence of acceptor (F_D),

$$E_t = 1 - \frac{F_{DA}}{F_D}. \quad (4)$$

Significant improvement in accuracy can be achieved if the energy transfer is calculated from a single sample, becoming then a differential measurement with an internal reference. In FRET this can be accomplished by calculating E_t from the ratio of the acceptor and donor peak intensities in the sample that contains both probes. To do that, one requires a calibration of the peak ratio to the energy transfer efficiency. This was achieved by examining a very large number of samples in several different lipid preparations of different compositions (Fig. 4). From these data, an empirical relation was found between the energy transfer efficiency and the fluorescence peak ratio (p_r) of NBD emission at 524 nm to MB emission at 460 nm,

$$E_t = \frac{6.66p_r^{2.33}}{1 + 6.66p_r^{2.33}} - 0.048. \quad (5)$$

Except in Fig. 4, all values of energy transfer efficiency reported here were calculated from this calibration curve.

Dependence of FRET on probe concentration in POPC and POPS membranes (effect of charge)

The goal of this work was to use the two probes, MB-POPE and NBD-POPE, to report on domain formation in BSM/Chol/POPC mixtures. One concern is that both probes carry negative charges at pH 7.5, so it is conceivable that repulsion between the two would decrease the energy transfer. To assess the effect of electrostatics on FRET, E_t was compared in vesicles of POPC (zwitterionic) and POPS (anionic) containing both probes at a fixed ratio of MB/NBD 1:1.5 and varying the MB-POPE concentration from 0.25 to 2 mol % of the lipid. The results, shown in Fig. 5, indicate that there is no difference between the two lipid matrices. Therefore, the effect of charge repulsion on the efficiency of energy transfer is negligible in these experiments.

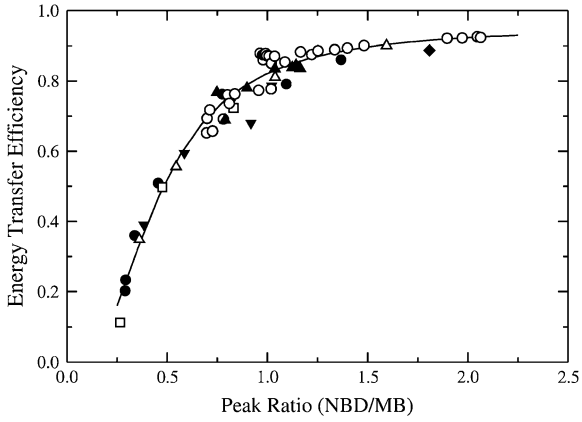

FIGURE 4 Experimental calibration of the energy transfer efficiency (E_t) with the NBD/MB peak ratio (p_r). For the calculation of peak ratios the intensities were read at 524 nm for NBD and 460 nm for MB (peak maxima). The FRET E_t was calculated from the intensity ratios of the MB peaks in samples containing both probes to identical samples containing only MB-POPE. These measurements were performed in a variety of lipid vesicles with different compositions and probe contents varying from 0.2 to 2 mol % relative to the total lipid. The different symbols correspond to experiments in the following lipid systems: POPC, open squares, solid diamonds, and solid triangles down; POPS, solid circles and open triangles; BSM/Chol/POPC 3:3:4, open circles; and BSM/Chol/POPC 4:4:2, solid triangles up. All points fall on the same curve, regardless of lipid composition and probe content of the vesicles. This curve can be empirically defined by the equation $E_t = (6.66p_r^{2.33})/(1+6.66p_r^{2.33}) - 0.048$, which is represented by the solid line.

Dependence of FRET on POPC mole fraction in BSM/Chol/POPC

The dependence of energy transfer efficiency on the mole fraction of POPC (X_{POPC}) in BSM/Chol/POPC vesicles was examined under two sets of conditions. First, the concentration of MB-POPE was kept at 1 mol % of the POPC content of the vesicles, and X_{POPC} was varied, maintaining the molar ratios BSM/Chol 1:1 and NBD/MB 1.5:1. The results are shown in Fig. 6, where E_t is plotted against X_{POPC} (*triangles*). The energy transfer efficiency increases with the POPC content of the vesicles and tends to a plateau.

Second, the concentration of MB-POPE was kept fixed at 0.5 mol % of the total lipid and X_{POPC} was varied, again maintaining the molar ratios BSM/Chol 1:1 and NBD/MB 1.5:1. A series of spectra for one of these experiments is shown in Fig. 7. FRET increases from *A* ($X_{POPC} = 0.20$) to *B* ($X_{POPC} = 0.40$) but then decreases in *C* ($X_{POPC} = 0.60$) and even more in panels *D* ($X_{POPC} = 0.80$) and *E* ($X_{POPC} = 1.0$). The observation of a maximum at $X_{POPC} \approx 0.30$–0.40 was consistently reproduced in all experiments where E_t was monitored as a function of X_{POPC} in mixtures of BSM/Chol/

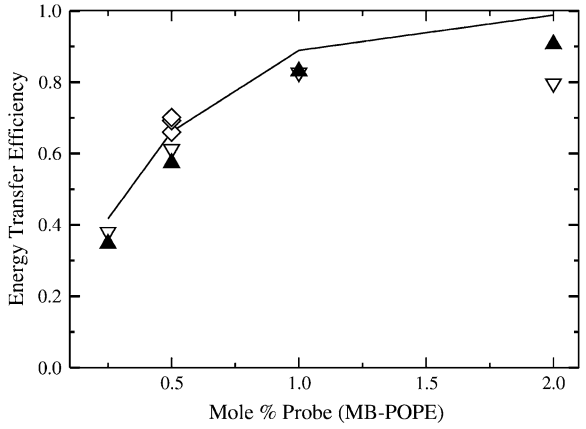

FIGURE 5 Dependence of E_t on the mol % of probe (MB-POPE) in LUVs of POPC (*open triangles*) and POPS (*solid triangles*). For POPC with 0.5 mol % MB-POPE three additional experiments are shown (*diamonds*) to convey the type of variance typically found in the experimental data. The acceptor/donor ratio is always NBD/MB = 1.5. The line represents the Monte Carlo simulation results calculated at 0.25, 0.5, 1.0, and 2.0 mol % MB-POPE, which are the same probe concentrations used in the experiments. The only adjustable parameter in the simulations is the experimental value of $R_0 = 46$ Å, which corresponds in the lattice to $R_0 = 6$ lipids for FRET within the same leaflet of the bilayer, or a projected value $R_0 = 2$ lipids for FRET across the bilayer.

POPC containing equimolar ratios of BSM and Chol. A plot of the energy transfer efficiency against the POPC concentration is shown in Fig. 8 (*circles*), corresponding to data from three independent experiments. On average, E_t goes

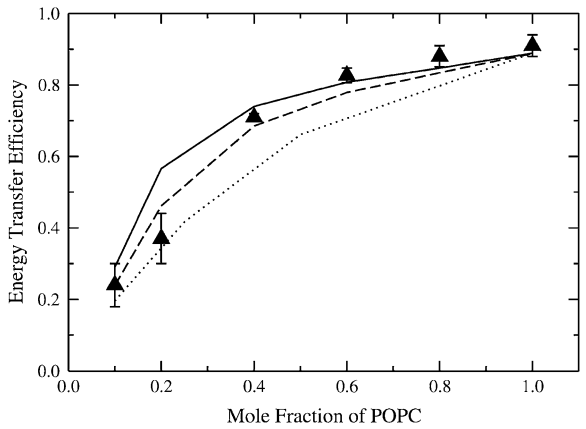

FIGURE 6 Dependence of E_t on X_{POPC} in LUVs of BSM/Chol/POPC with compositions 45:45:10, 40:40:20, 30:30:40, 20:20:60, 10:10:80, and pure POPC (*triangles*). Each data point shown is the average of two independent samples and the error bars are the corresponding standard deviations (in one case, hidden in the symbol). The MB-POPE probe concentrations are always 1 mol % of the POPC content and the ratio NBD/MB = 1.5. The solid line represents the Monte Carlo simulation results calculated for the same lipid compositions and probe concentrations, using the parameters $\omega_{SC} = -350$, $\omega_{SP} = 300$, and $\omega_{CP} = 200$ cal/mol. The dashed line corresponds to a calculation where ω_{SP} was changed to 250 cal/mol. The dotted line in Fig. 6 is the same calculation as the line in Fig. 5, corresponding to pure POPC, where no domains exist.

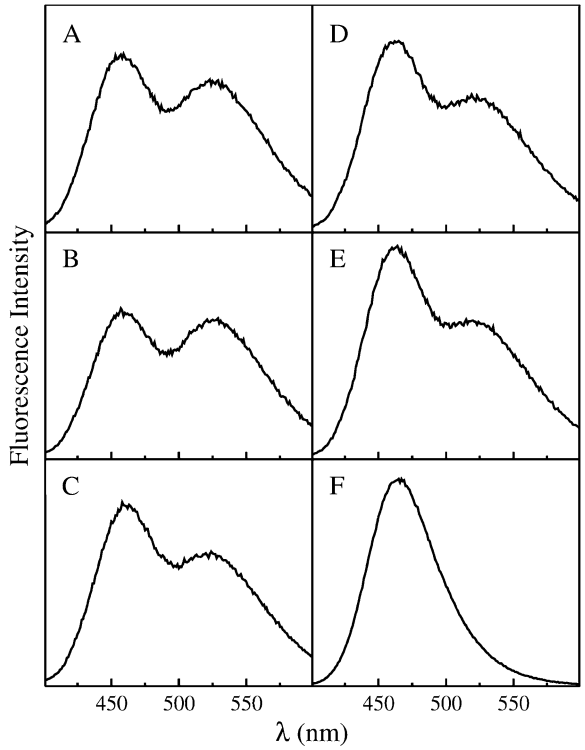

FIGURE 7 Representative series of spectra recorded in one experiment where the POPC mole fraction was varied in BSM/Chol/POPC mixtures, while keeping an equimolar ratio of BSM/Chol. (*A*) $X_{POPC} = 0.20$, (*B*) 0.40, (*C*) 0.60, (*D*) 0.80, and (*E*) pure POPC. All spectra *A–E* are shown on the same vertical scale and contain 0.5 mol % MB-POPE and 0.75 mol % NBD-POPE (NBD/MB = 1.5). For reference, (*F*) shows the spectrum of a sample containing only donors (MB-POPE). The vertical scale in (*F*) is ~3× larger than in the other spectra, that is, the MB peak in (*F*) is really ~3× larger. The total lipid concentrations are the same in all samples (100 μM).

through a maximum at $X_{POPC} \approx 0.30$. This clearly indicates that lipid domains exist in this system. Otherwise, E_t would be independent of X_{POPC}. These two experiments, especially the second, which is much more sensitive, were used to refine the estimates of the unlike lipid-lipid interaction Gibbs energies in the Monte Carlo simulations.

Monte Carlo simulations and domain sizes

Monte Carlo simulations on a lattice were used to interpret the experimental values of energy transfer efficiency. In these simulations the lipid bilayer is represented by two superimposed triangular matrices, each site representing a lipid. The probes behave as tagged POPC molecules in their interactions with other lipids. In addition, energy transfer occurs if an acceptor (NBD-POPE) is within the distance, R_0, of a donor (MB-POPE). In the simulations, this distance corresponds to 6 lipids (~46 Å) if donor and acceptor are in the same leaflet or 2 lipids (projected distance) if they are in opposite leaflets of the bilayer. Using these distances and no

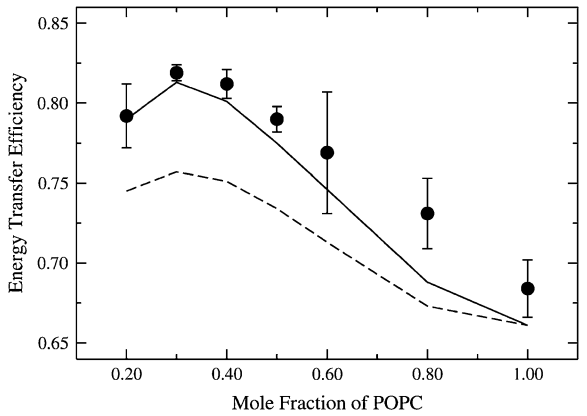

FIGURE 8 Dependence of E_t on X_{POPC} in LUVs of BSM/Chol/POPC. FRET experiments (*solid circles*) were performed on vesicles with the following compositions, all of which have equimolar mixtures of SM and Chol (letters in parenthesis correspond to the panels in Fig. 7): SM/Chol/POPC 40:40:20 (*A*), 35:35:30, 30:30:40 (*B*), 25:25:50, 20:20:60 (*C*), 10:10:80 (*D*), and pure POPC (*E*). The MB-POPE probe concentrations are kept fixed at 0.5 mol % of the total lipid, and the ratio NBD/MB = 1.5. Each point represents the average of three independent experiments (two for $X_{POPC} = 0.30$ and 0.50) and the error bars are the standard deviations. The solid line represents the Monte Carlo simulation results calculated for the same lipid compositions and probe concentrations, using the parameters $\omega_{SC} = -350$, $\omega_{SP} = 300$, and $\omega_{CP} = 200$ cal/mol. The dashed line corresponds to a calculation where ω_{SP} was changed to 250 cal/mol.

other adjustable parameters, the Monte Carlo simulations agree well with the experimental dependence of FRET on the probe concentration in pure POPC and in pure POPS membranes, as shown by the line in Fig. 5. Although for the two complete experiments shown for POPS (*solid triangles*) and POPC (*open triangles*) the calculations appear to be systematically high, they actually match exactly three other sets of data obtained at 0.5 mol % in POPC (*open diamonds*). The small difference between the simulations and the data in general is not any larger than the dispersion in the experiments from independent data sets.

When simulating mixtures, three unlike nearest-neighbor interaction parameters must be included: ω_{SP} for SM/POPC, ω_{SC} for SM/Chol, and ω_{CP} for Chol/POPC interactions. As described in the Introduction, the choice of the values for these parameters was guided by experimental data available and by previous Monte Carlo simulations, which were themselves performed trying to match experimental results. Beyond those considerations, the impact of these parameters on the results of the simulations was extensively tested. In these tests, the experimental values of energy transfer efficiency were a guide to the correctness of the choice of parameters. The choice of $\omega_{SC} = -350$, $\omega_{SP} = +300$, and $\omega_{CP} = +200$ cal/mol yielded the best overall agreement between the FRET experiments and the Monte Carlo simulations, as shown by the solid lines in Fig. 6 and, especially, in Fig. 8. The sensitivity of the calculations to the interaction parameters can be inferred from the dashed lines in Figs. 6 and 8, which correspond to $\omega_{SP} = 250$ instead of 300 cal/mol, keeping the other parameters the same. The dotted line in Fig. 6 is the same as the line in Fig. 5, corresponding to pure POPC, where no domains exist. Comparison between the solid and dotted lines in Fig. 6 shows the effect of domains on FRET in this experiment. However, some parameter correlation is observed; as long as $\omega_{CP} + \omega_{SP} - \omega_{SC} \approx 850$ cal/mol, the first two being positive and the third negative, it is possible to fit the data quite well. Using those parameter values, the differences between the experimental and calculated points are never larger that the dispersion in the experimental data, perhaps with the exception of the point corresponding to $X_{POPC} = 0.20$ in Fig. 6. Overall, the calculations reproduce well the values of E_t. But perhaps the strongest support for the correctness of the essential features of the simulations is that they reproduce the shape of the dependence of E_t on X_{POPC} (Fig. 8), a result that is nontrivial.

Having calibrated the Monte Carlo simulations with the FRET experiments, it is now possible to extract information regarding lipid domain sizes from the calculations. A snapshot of one of the monolayers for an equilibrated bilayer with the composition SM/Chol/POPC 35:35:30 is shown in Fig. 9 *A*. This picture is typical of the most common lattice configuration observed with the interaction parameters $\omega_{SC} = -350$, $\omega_{SP} = +300$, and $\omega_{CP} = +200$ cal/mol. In this snapshot, a large domain is observed, which coexists with a few intermediate ones, but mainly with small domains of ~10 molecules or less. This is more clearly seen by examining the distribution of POPC molecules in domains of different sizes shown in Fig. 10 (*black*), which is cumulative for an entire Monte Carlo run. This distribution is highly asymmetric: many small domains coexist with one or two very large ones. Essentially a phase separation occurs between a SM/Chol 1:1 domain and a POPC domain. The large domain contains ~2,300 POPC lipids, ~3/4 of the total POPC in a lattice of 100 × 100 sites with $X_{POPC} = 0.30$.

To examine the effect of lattice size on the domain distribution function, a few simulations were performed on a 300 × 300 lattice, which has the number of lipids of a real LUV, the experimental model system investigated. Most often, one large POPC domain is formed, which coexists with many small ones. The distribution function for SM/Chol/POPC 35:35:30 shows that this domain contains ~21,000 POPC lipids, again ~3/4 of the total POPC in the lattice. This corresponds to an extensive phase separation. To examine the sensitivity of the calculations to the interaction parameters and the lattice size, simulations were performed in both lattices with $\omega_{SC} = -350$ and $\omega_{CP} = +200$ cal/mol, but varying ω_{SP} from 300 down to 250 cal/mol. The domain size distribution function changes already with $\omega_{SP} = 270$ cal/mol (Fig. 10, *red*), no longer showing a complete phase separation, but a broad maximum centered around 1,900 lipids in the 100 × 100 lattice and around 7,000 lipids in the 300 × 300 lattice, which corresponds to only ~1/4 of the POPC. With $\omega_{SP} = 250$ cal/mol (Fig. 10, *green*), the distribution

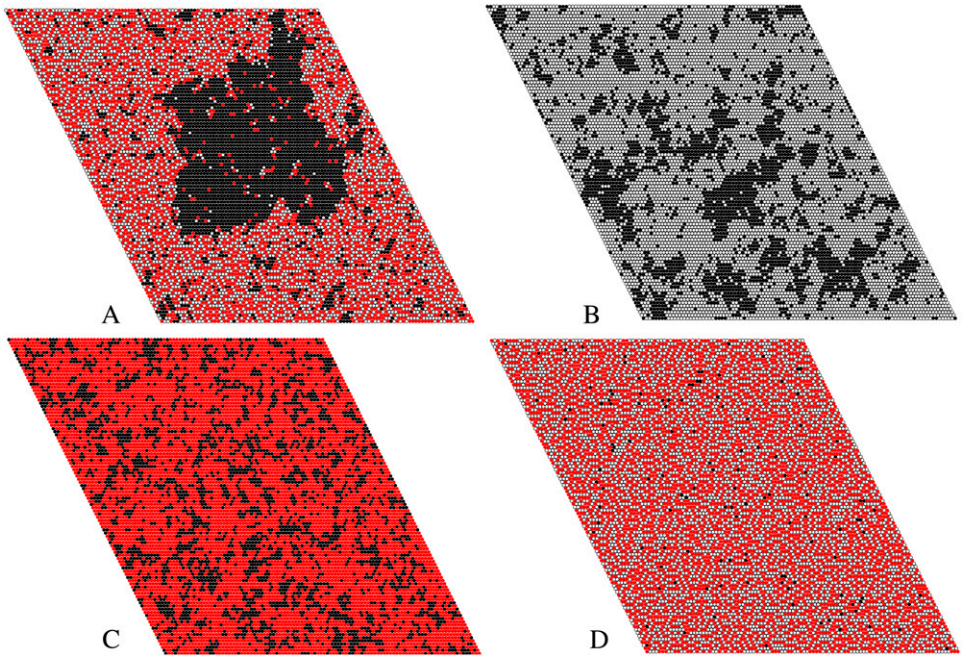

FIGURE 9 Snapshot of one monolayer of an equilibrated Monte Carlo simulation of (*A*) SM/Chol/POPC 35:35:30, (*B*) SM/POPC 70:30, (*C*) Chol/POPC 70:30, and (*D*) SM/Chol 50:50. POPC molecules are represented by the black lattice sites, Chol molecules are represented by the red sites, and SM molecules are represented by the white sites. The lattice size was 100 × 100 (10,000 lipids) and the lipid-lipid interaction parameters were $\omega_{SC} = -350$, $\omega_{SP} = +300$, and $\omega_{CP} = +200$ cal/mol in this simulation. In (*D*) the few black sites are the probes.

looks completely different, showing essentially an exponential decay with domain size and no phase separation in either lattice. A snapshot of the 100 × 100 lattice for a calculation with $\omega_{SP} = 250$ cal/mol is shown in Fig. 11. Equivalent changes in domain sizes are observed if one of the other two parameters, or a combination of the three, is reduced in absolute value by 30–50 cal/mol. Finally, with the same parameters, the values calculated for the energy transfer efficiency (E_t) are larger by ~1%–2% in the 300 × 300 lattice. This means that, to obtain the same experimental values of E_t, slightly smaller parameters, in absolute value, could be used in the 300 × 300 lattice.

DISCUSSION

Domain formation in mixtures of BSM/Chol/POPC was investigated by a combination of experimental FRET measurements and Monte Carlo simulations. FRET occurs between two probes, MB-POPE and NBD-POPE, the acyl chains of which are identical to those of POPC and POPS. Therefore, these probes are expected to behave much more similarly to POPC than to SM or Chol. FRET was examined in BSM/Chol/POPC mixtures with a ratio of BSM/Chol 1:1 and

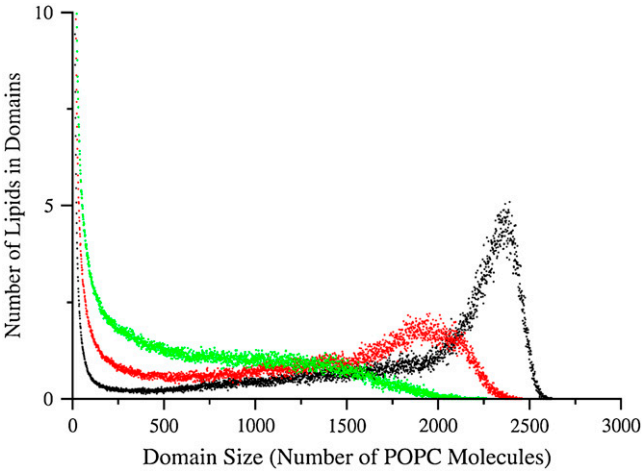

FIGURE 10 Distribution of domain sizes in a Monte Carlo simulation on a 100 × 100 lattice. Clusters of ≥2 POPC sites are counted in the distribution. The unlike, lipid-lipid interaction parameters are $\omega_{SC} = -350$ cal/mol, $\omega_{CP} = +200$ cal/mol, and ω_{SP} varied: 300 cal/mol (*black*), 270 cal/mol (*red*), and 250 cal/mol (*green*).

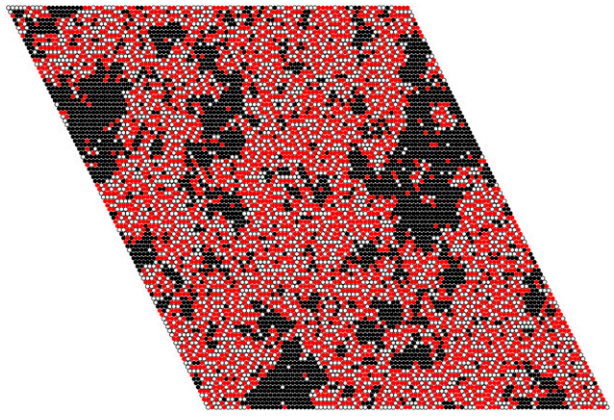

FIGURE 11 Snapshot of one monolayer of an equilibrated Monte Carlo simulation of SM/Chol/POPC 35:35:30. Notation and parameters are as in Fig. 9, except that $\omega_{SP} = +250$ cal/mol, reduced by 50 cal/mol relative to the simulation of Fig. 9 *A*, with which this snapshot should be compared.

variable POPC content. Samples of pure POPC and pure POPS containing the probes were also examined and showed identical behavior, indicating that electrostatic effects or other headgroup interactions have a negligible influence on the observed FRET. If these effects were significant, repulsion between the two anionic probes would be expected to be larger in POPC (zwitterionic) than in POPS (anionic), which should mask the probes. In that case, a lower FRET should be observed in POPC compared to POPS. However, FRET is identical in both lipid matrices (Fig. 5).

When the POPC content is increased in mixtures of BSM/Chol/POPC with equimolar amounts of BSM and Chol while increasing the probe concentration in the same proportion, FRET increases, tending to a plateau (Fig. 6). When the POPC content is increased, but keeping the probe concentration fixed with respect to the total lipid, the energy transfer efficiency (E_t) goes through a maximum at $X_{POPC} \sim 0.30$ (Fig. 8). This clearly indicates that domains exist in these mixtures; otherwise, if mixing were ideal, a constant value of E_t would be observed. Qualitatively, we interpret the occurrence of this maximum as the result of two different processes. At low X_{POPC} (≤ 0.20), POPC exists mainly in small domains; POPC molecules and the probes are therefore dispersed in the SM/Chol matrix, with relatively few donor/acceptor pairs in the same domains. As X_{POPC} increases, larger domains exist and more probe pairs reside in the same domains, so FRET increases. However, as X_{POPC} increases even further, because in this experiment the probe concentration is fixed relative to the total lipid, the probes are diluted out within the POPC domains and FRET decreases.

To obtain a quantitative interpretation of those results, Monte Carlo simulations were performed on two superimposed triangular lattices, which represent the lipid bilayer. The two lattices were necessary to account for energy transfer across the bilayer, which occurs because of the large Förster distance of this donor/acceptor pair, $R_0 = 46$ Å. Using this experimental parameter and the thickness of the lipid bilayer (65), and no adjustable parameters, the Monte Carlo simulations reproduced well the FRET observed in pure POPC (Fig. 5). In simulations of SM/Chol/POPC mixtures, the unlike lipid-lipid interaction Gibbs energies need to be included. The approximate values of those interaction parameters were based on experimental data as much as possible and then fine-tuned by comparing the experimentally observed FRET with its value calculated in Monte Carlo simulations. The values that yielded the overall best agreement between data and simulations were $\omega_{SC} = -350$ cal/mol for SM/Chol, $\omega_{SP} = +300$ cal/mol for SM/POPC, and $\omega_{CP} = +200$ cal/mol for Chol/POPC interaction. These parameters indicate that there is a slight repulsive interaction between Chol and POPC, but so little that it would be hard to distinguish from random mixing (Fig. 9 *C*); a stronger repulsive interaction between SM and POPC (Fig. 9 *B*); and a favorable interaction between SM and Chol (Fig. 9 *D*). This might be sufficient to explain observations that have been interpreted as the formation of condensed complexes between phospholipids and Chol (4,13,30). It is, however, also consistent with the existence of L_o phase or domains. The snapshot of a Monte Carlo simulation of SM/Chol/POPC 35:35:30, shown in Fig. 9 *A*, makes these comments evident. On the one hand, Chol molecules (*red*) appear usually paired with SM molecules (*white*), giving the impression of a complex. On the other hand, extensive regions of SM/Chol (L_o) coexist with large POPC domains (L_d).

For $X_{POPC} = 0.30$, the POPC domain distribution consists of one large domain (occasionally two), which contains ~3/4 of the POPC lipids, and many small ones with ~10 lipids or fewer (Fig. 10) in both 100×100 and 300×300 lattices. The largest POPC domains would have real linear dimensions of the order of a few hundred nanometers. These sizes are too small to be observed by fluorescence microscopy and indeed they have not been observed by this method (26). However, they are large enough to be detected by FRET. They are also large enough to have a significant effect on the interaction of peptides and peripheral proteins with membranes. Indeed, the kinetics of the interaction of the peptide δ-lysin with vesicles of BSM/Chol/POPC are strongly dependent on the fractions of L_d and L_o domains (1). On that basis, we have proposed a phase diagram for BSM/Chol/POPC (1). We conjectured then that the domains must be at least larger than the peptide length (4 nm) to be detected. The conclusions reached here are consistent with that idea.

Nevertheless, if the scaling of domain size with lattice size were exact, ~3/4 of the lipid in a GUV with a composition BSM/Chol/POPC ~1:1:1 would form a domain that would be visible by fluorescence microscopy. Simulating a lattice with a size corresponding to a GUV is beyond our present capacity. However, a comparison of the effect of the unlike lipid-lipid interaction parameters on the domain distribution functions in 100×100 and 300×300 lattices indicates that scaling with lattice size is approximate but not exact. This is because the entropy gain from splitting a large domain into smaller ones is greater in the larger lattice. Thus, as the lattice size increases, the domain size increases as well, but not in the same proportion. Furthermore, slightly smaller parameters in the 300×300 lattice are sufficient to produce the same effect on the calculated FRET in comparison with the 100×100 lattice. This suggests that the real parameters might be slightly smaller in absolute value. In a GUV, the distribution would be even further shifted to smaller domains. To produce good agreement with experiment, the absolute values of the unlike lipid-lipid interaction Gibbs energies, ω_{SP}, ω_{CP}, and ω_{SC}, must add up to 850 cal/mol. Very small decreases in the absolute value of any of these three parameters, by as little as 50 cal/mol, lead to a change from phase separation to small domains (compare Figs. 9 *A* and 11). It is also possible that the unlike lipid-lipid interaction Gibbs energies are actually somewhat smaller in a GUV than in a LUV. This would further enhance the tendency for small domains in GUVs of this BSM/Chol/

POPC mixture, in agreement with the fluorescence microscopy results (26), and is perhaps one of the reasons there is some discrepancy in observations of large phase separation or not when these mixtures are investigated in different vesicle systems.

Finally, the simulations presented here shed some light on the observation that whereas binary mixtures of SM/Chol, SM/POPC, and Chol/POPC do not show macroscopic phase separation by fluorescence microscopy of GUVs, some of these ternary mixtures do, leading to a closed loop in the ternary phase diagram (3,66), as illustrated in Fig. 1. Examination of Fig. 9 clearly shows that a closed loop occurs in the phase diagram. In Fig. 9 *A*, phase separation is observed in the ternary mixture SM/Chol/POPC 35:35:30. But in Fig. 9 *B* (SM/POPC 70:30), *C* (Chol/POPC 70:30), and *D* (SM/Chol 1:1), where the pairs of components have been combined in binary mixtures containing the same amount of POPC as in Fig. 9 *A* or equimolar amounts of SM and Chol, no massive phase separation is observed. Thus, all that is required for the observation of a closed loop in the ternary phase diagram is a strong, favorable interaction between SM and Chol and two weak, unfavorable interactions between Chol and POPC and between SM and POPC. When SM and Chol are paired they maintain the same interactions with each other and with POPC as they have in the absence of pair formation. That is, when adjacent to Chol, SM does not have a different interaction with POPC than what it has in the absence of Chol. Thus, there is no need to involve multibody interactions to explain these properties of ternary mixtures of SM/Chol/POPC; three pairs of binary interactions (ω_{AB}) are sufficient.

McConnell and his collaborators have proposed a model that explains those experimental observations by the formation of SM-Chol condensed complexes, which have a repulsive interaction with POPC (4,13,30,66). In this model, SM/Chol binary mixtures would not show phase separation. These ideas are compatible with the results of the Monte Carlo simulations presented here, with the parameter values used, and within the approximation of our simple model, which has only one state for SM (L_o). The condensed complex model uses regular solution theory and selects as key chemical components the complex and the disordered lipid (POPC). The interactions between these components—the equilibrium constant for complex formation and the repulsion between complex and POPC—then, together with the mixing entropy, determine the properties of the system. Perhaps the main difference between the two models is the magnitude of the (Gibbs) energies of the interactions involved. The repulsion between a SM-Chol condensed complex and POPC is similar to the average repulsion between a SM-Chol pair and POPC in our model. But the interaction between SM and Chol is only −350 cal/mol in our model, whereas the equilibrium constant for formation of a condensed complex corresponds to a Gibbs energy of −3 kcal/mol (66) at room temperature. The enthalpy of formation of a condensed complex is about −9 kcal/mol (66), whereas the experimentally determined temperature dependence of ω_{AB} for DPPC/Chol in the L_o phase is only −2 kcal/mol (39). The high values of the energies in the condensed complex model are probably, in part, a consequence of using regular solution theory, which overestimates the mixing entropy and may therefore require large energy values to compensate for it.

We thank Alexis Oldham for performing a few of the experiments.

This work was supported in part by Cottrell College Science Award CC6246 from the Research Corporation and by Grant GM072507 from the National Institutes of Health.

REFERENCES

1. Pokorny, A., L. E. Yandek, A. I. Elegbede, A. Hinderliter, and P. F. F. Almeida. 2006. Temperature and composition dependence of the interaction of δ-lysin with ternary mixtures of sphingomyelin/cholesterol/POPC. *Biophys. J.* 91:2184–2197.
2. de Almeida, R. F. M., A. Fedorov, and M. Prieto. 2003. Sphingomyelin/phosphatidylcholine/cholesterol phase diagram: boundaries and composition of lipid rafts. *Biophys. J.* 85:2406–2416.
3. Veatch, S. L., and S. L. Keller. 2005. Miscibility phase diagrams of giant vesicles containing sphingomyelin. *Phys. Rev. Lett.* 94:148101.
4. McConnel, H. 2005. Complexes in ternary cholesterol–phospholipid mixtures. *Biophys. J.* 88:L23–L25.
5. Elliott, R., I. Szleifer, and M. Schick. 2006. Phase diagram of a ternary mixture of cholesterol and saturated and unsaturated lipids calculated from a microscopic model. *Phys. Rev. Lett.* 96:098101.
6. Cullis, P. R., and M. J. Hope. 1985. Physical properties and functional roles of lipids in membranes. *In* Biochemistry of Lipids and Membranes. D. E. Vance and J. E. Vance, editors. Benjamin/Cummings, Menlo Park, CA. 28–33.
7. Zachowski, A. 1993. Phospholipids in animal eukaryotic membranes: transverse asymmetry and movement. *Biochem. J.* 234:1–14.
8. Ahmed, S. N., D. A. Brown, and E. London. 1997. On the origin of sphingolipid/cholesterol-rich detergent-insoluble cell membranes: physiological concentrations of cholesterol and sphingolipid induce formation of a detergent-insoluble, liquid-ordered lipid phase in model membranes. *Biochemistry.* 36:10944–10953.
9. McMullen, T. P. W., R. N. A. H. Lewis, and R. N. McElhaney. 2004. Cholesterol-phospholipid interactions, the liquid-ordered phase and lipid rafts in model and biological membranes. *Current Opin. Colloid Interface Sci.* 8:459–468.
10. Simons, K., and E. Ikonen. 1997. Functional rafts in cell membranes. *Nature.* 387:569–572.
11. Brown, D. A., and E. London. 1998. Functions of lipid rafts in biological membranes. *Annu. Rev. Cell Dev. Biol.* 14:111–136.
12. Edidin, M. 2003. The state of lipid rafts: from model membranes to cells. *Annu. Rev. Biophys. Biomol. Struct.* 32:257–283.
13. McConnell, H. M., and M. Vrljic. 2003. Liquid-liquid immiscibility in membranes. *Annu. Rev. Biophys. Biomol. Struct.* 32:469–492.
14. Simons, K., and W. L. Vaz. 2004. Model systems, lipid rafts, and cell membranes. *Annu. Rev. Biophys. Biomol. Struct.* 33:269–295.
15. Brown, D. A., and E. London. 1997. Structure of detergent-resistant membrane domains: does phase separation occur in biological membranes? *Biochem. Biophys. Res. Commu.* 240:1–7.
16. Samsonov, A. V., I. Mihalyov, and F. S. Cohen. 2001. Characterization of cholesterol-sphingomyelin domains and their dynamics in bilayer membranes. *Biophys. J.* 81:1486–1500.
17. Rietveld, A., and K. Simons. 1998. The differential miscibility of lipids as the basis for the formation of functional membrane rafts. *Biochim. Biophys. Acta.* 1376:467–479.

18. Dietrich, C., L. A. Bagatolli, Z. N. Volovyk, N. L. Thompson, M. Levi, K. Jacobson, and E. Gratton. 2001. Lipid rafts reconstituted in model membranes. *Biophys. J.* 80:1417–1428.

19. Ipsen, J. H., G. Karlstroem, O. G. Mouritsen, H. Wennerstroem, and M. J. Zuckermann. 1987. Phase equilibria in the phosphatidylcholine-cholesterol system. *Biochim. Biophys. Acta.* 905:162–172.

20. Ipsen, J. H., O. G. Mouritsen, and M. J. Zuckermann. 1989. Theory of thermal anomalies in the specific heat of lipid bilayers containing cholesterol. *Biophys. J.* 56:661–667.

21. Sankaram, M. B., and T. E. Thompson. 1990. Interaction of cholesterol with various glycerophospholipids and sphingomyelin. *Biochemistry.* 29:10670–10675.

22. Collado, M. I., F. M. Goñi, A. Alonso, and D. Marsh. 2005. Domain formation in sphingomyelin/cholesterol mixed membranes studied by spin-label electron spin resonance spectroscopy. *Biochemistry.* 44: 4911–4918.

23. Bacia, K., D. Scherfeld, N. Kahya, and P. Schwille. 2004. Fluorescence correlation spectroscopy relates rafts in model and native membranes. *Biophys. J.* 87:1034–1043.

24. Kahya, N., D. Scherfeld, K. Bacia, B. Poolman, and P. Schwille. 2003. Probing lipid mobility of raft-exhibiting model membranes by fluorescence correlation spectroscopy. *J. Biol. Chem.* 278:28109–28115.

25. de Almeida, R. F. M., L. M. S. Loura, A. Fedorov, and M. Prieto. 2005. Lipid rafts have different sizes depending on membrane composition: a time-resolved fluorescence resonance energy transfer study. *J. Mol. Biol.* 346:1109–1120.

26. Veatch, S. L., and S. L. Keller. 2003. Separation of liquid phases in giant vesicles of ternary mixtures of phospholipids and cholesterol. *Biophys. J.* 85:3074–3083.

27. Pokorny, A., and P. F. F. Almeida. 2005. Permeabilization of raft-containing lipid vesicles by δ-lysin: a mechanism for cell sensitivity to cytotoxic peptides. *Biochemistry.* 44:9538–9544.

28. Silvius, J. R. 2003. Fluorescence energy transfer reveals microdomain formation at physiological temperatures in lipid mixtures modeling the outer leaflet of the plasma membrane. *Biophys. J.* 85:1034–1045.

29. Feigenson, G. W., and J. T. Buboltz. 2001. Ternary phase diagram of dipalmitoyl-PC/dilauroyl-PC/cholesterol: nanoscopic domain formation driven by cholesterol. *Biophys. J.* 80:2775–2788.

30. McConnell, H. M., and A. Radhakrishnan. 2003. Condensed complexes of cholesterol and phospholipids. *Biochim. Biophys. Acta.* 1610: 159–173.

31. Almeida, P. F. F., A. Pokorny, and A. Hinderliter. 2005. Thermodynamics of membrane domains. *Biochim. Biophys. Acta.* 1720:1–13.

32. Krisovitch, S. M., and S. L. Regen. 1992. Nearest-neighbor recognition in phospholipid membranes: a molecular-level approach to the study of membrane suprastructure. *J. Am. Chem. Soc.* 114:9828–9835.

33. Davidson, S. M. K., and S. L. Regen. 1997. Nearest-neighbor recognition in phospholipid membranes. *Chem. Rev.* 97:1269–1279.

34. Vigmond, S. J., T. Dewa, and S. L. Regen. 1995. Nearest-neighbor recognition within a mixed phospholipid membrane: evidence for lateral heterogeneity. *J. Am. Chem. Soc.* 117:7838–7839.

35. Dewa, T., S. J. Vigmond, and S. L. Regen. 1996. Lateral heterogeneity in fluid bilayers composed of saturated and unsaturated phospholipids. *J. Am. Chem. Soc.* 118:3435–3440.

36. Sugahara, M., M. Uragami, and S. L. Regen. 2002. Selective sterol-phospholipid associations in fluid bilayers. *J. Am. Chem. Soc.* 124: 4253–4256.

37. Sugahara, M., M. Uragami, and S. L. Regen. 2003. Selective association of cholesterol with long-chain phospholipids in liquid-ordered bilayers: support for the existence of lipid rafts. *J. Am. Chem. Soc.* 125:13040–13041.

38. Tokutake, N., B. Jing, and S. L. Regen. 2003. Detection of unusual lipid mixing in cholesterol-rich phospholipid bilayers: the long and the short of it. *J. Am. Chem. Soc.* 125:8994–8995.

39. Zhang, J., H. Cao, B. Jing, P. F. Almeida, and S. L. Regen. 2006. Cholesterol-phospholipid association in fluid bilayers: a thermodynamic analysis from nearest-neighbor recognition measurements. *Biophys. J.* 91:1402–1406.

40. Hinderliter, A., P. F. F. Almeida, C. E. Creutz, and R. L. Biltonen. 2001. Domain formation in a fluid mixed lipid bilayer modulated through binding of the C2 protein motif. *Biochemistry.* 40:4181–4191.

41. Hinderliter, A., R. L. Biltonen, and P. F. F. Almeida. 2004. Lipid modulation of protein-induced membranes domains as a mechanism for controlling signal transduction. *Biochemistry.* 43:7102–7110.

42. Sugar, I. P., T. E. Thompson, and R. L. Biltonen. 1999. Monte Carlo simulation of two-component bilayers: DMPC/DSPC mixtures. *Biophys. J.* 76:2099–2100.

43. Jerala, R., P. F. F. Almeida, and R. L. Biltonen. 1996. Simulation of the gel-fluid transition in a membrane composed of lipids with two connected acyl chains: application of a dimer-move step. *Biophys. J.* 71:609–615.

44. Sugar, I. P., R. L. Biltonen, and N. Mitchard. 1994. Monte Carlo simulation of membranes: phase transition of small unilamellar dipalmitoylphosphatidylcholine vesicles. *Meth. Enzymol.* 240:569–593.

45. Parsegian, V. A. 1995. The cows or the fence? *Mol. Membr. Biol.* 12:5–7.

46. Silvius, J. R. 2003. Role of cholesterol in lipid raft formation: lessons from lipid model systems. *Biochim. Biophys. Acta.* 1610:174–183.

47. Ohvo-Rekilä, H., B. Ramstedt, P. Leppimäki, and J. P. Slotte. 2002. Cholesterol interaction with phospholipids in membranes. *Prog. Lipid Res.* 41:66–97.

48. Niu, S.-L., and B. J. Litman. 2002. Determination of membrane cholesterol partition coefficient using a lipid vesicle-cyclodextrin binary system: effect of phospholipid acyl chain unsaturation and headgroup composition. *Biophys. J.* 83:3408–3415.

49. Harroun, T. A., J. Katsaras, and S. R. Wassall. 2006. Cholesterol hydroxyl group is found to reside in the center of a polyunsaturated lipid membrane. *Biochemistry.* 45:1227–1233.

50. Mateo, R. C., A. U. Acuña, and J.-C. Brochon. 1995. Liquid-crystalline phases of cholesterol/lipid bilayers as revealed by the fluorescence of *trans*-parinaric acid. *Biophys. J.* 68:978–987.

51. Henriksen, J., A. C. Rowat, E. Brief, Y. W. Hsueh, J. L. Thewalt, M. J. Zuckermann, and J. H. Ipsen. 2006. Universal behavior of membranes with sterols. *Biophys. J.* 90:1639–1649.

52. Heimburg, T., and R. L. Biltonen. 1996. A Monte Carlo simulation study of protein-induced heat capacity changes and lipid-induced protein clustering. *Biophys. J.* 70:84–96.

53. Bartlett, G. R. 1959. Phosphorous assay in column chromatography. *J. Biol. Chem.* 234:466–468.

54. Pokorny, A., T. H. Birkbeck, and P. F. F. Almeida. 2002. Mechanism and kinetics of δ-lysin interaction with phospholipid vesicles. *Biochemistry.* 41:11044–11056.

55. Vaz, W. L. C., and D. Hallmann. 1983. Experimental evidence against the applicability of the Saffman-Delbrück model to the translational diffusion of lipids in phosphatidylcholine bilayer membranes. *FEBS Lett.* 152:287–290.

56. Kates, M. 1972. Techniques in lipidology. *In* Laboratory Techniques in Biochemistry and Molecular Biology. T. S. Work and E. Work, editors. North-Holland Publishing Company, Amsterdam. 421.

57. Lakowicz, J. R. 1999. Principles of Fluorescence Spectroscopy, 2nd ed. Kluwer, New York.

58. Sun, W.-C., K. R. Gee, and R. P. Haugland. 1998. Synthesis of novel fluorinated coumarins: excellent UV-light excitable fluorescent dyes. *Bioorg. Med. Chem. Lett.* 8:3107–3110.

59. Haugland, R. P. 2002. Handbook of Fluorescence Probes and Research Products, 9th ed. Molecular Probes, Eugene, OR.

60. Binder, K., and D. W. Heermann. 1997. Monte Carlo Simulation in Statistical Physics, 3rd ed. Springer, New York.

61. Kawasaki, K. 1972. Kinetics of Ising models. *In* Phase Transitions and Critical Phenomena, Vol. 2. C. Domb and M. S. Green, editors. Academic Press, New York. 443–501.

62. Press, W. H., S. A. Teukolsky, W. T. Vetterling, and B. P. Flannery. 1994. Numerical Recipes in FORTRAN: The Art of Scientific Computing, 2nd ed. Cambridge University Press, Cambridge.

63. Metropolis, N., A. W. Rosenbluth, W. N. Rosenbluth, A. H. Teller, and E. Teller. 1953. Equation of state calculations by fast computing machines. *J. Chem. Phys.* 21:1087–1092.

64. Abreu, M. S. C., M. J. Moreno, and W. L. C. Vaz. 2004. Kinetics and thermodynamics of association of a phospholipid derivative with lipid bilayers in liquid-disordered and liquid-ordered phases. *Biophys. J.* 87:353–365.

65. Wiener, M. C., and S. H. White. 1992. Structure of a fluid dioleoylphosphatidylcholine bilayer determined by joint refinement of x-ray and neutron diffraction data. III. Complete structure. *Biophys. J.* 61:437–447.

66. Radhakrishnan, A., and H. McConnell. 2005. Condensed complexes in vesicles containing cholesterol and phospholipids. *Proc. Natl. Acad. Sci. USA.* 102:12662–12666.